Nanoscale

PAPER

View Article Online
View Journal | View Issue

Cite this: *Nanoscale*, 2025, **17**, 20445

Size and softness synergy in cellular microgel uptake: a force spectroscopy study

Andrey Babenyshev, [a] Victoria K. Switacz, [b] Marc Spehr [b] and Walter Richtering *[a]

Received 24th June 2025,
Accepted 14th August 2025

DOI: 10.1039/d5nr02681d

rsc.li/nanoscale

Poly(*N*-isopropylacrylamide) (PNIPAM) microgels hold promise for various biomedical applications, yet the mechanisms governing microgel interactions with cells remain poorly understood. Recent studies have highlighted the influence of cross-linker content and microgel size on cellular uptake. In this study, we employed atomic force microscopy to systematically investigate the internal structure of both conventional and ultralow cross-linked (ULC) PNIPAM microgels physically adsorbed at the glass/water interface. By studying the correlation between the degree of microgel deformation on a rigid substrate and their stiffness, measured *via* force spectroscopy, we developed a characterization method that predicts microgel uptake ability in HEK293T cells. Notably, our findings extend to micron-sized ULC microgels, validating the proposed concept. Together, our approach enables the prediction of cellular internalization across a wide range of microgel types, potentially streamlining the screening of crucial microgel properties during early synthesis stages, prior to extensive cell interaction experiments.

1. Introduction

In recent decades, nanomaterials have emerged as promising candidates for biomedical applications.[1] These materials, from metallic nanoparticles (NPs) to polymeric carriers, have improved conventional disease treatments by enabling targeted delivery, controlled release, and enhanced therapeutic efficacy. Among the diverse array of nanocarriers, microgels form a unique class. These aqueous cross-linked polymeric particles with tunable size, easy to functionalize porous networks allowing encapsulation, and excellent biocompatibility emerge as versatile platforms for drug delivery.[2–8]

To optimize nanomaterial-based delivery systems, rational design requires consideration of multiple parameters. Key considerations include specificity to target tissues, delivery efficiency, and minimization of side effects. These factors are intimately linked to the physicochemical properties of the carriers.[9,10] The ability to tune such properties has advanced targeted drug delivery, yet there is still a lack of comprehensive understanding of how carrier properties influence their therapeutic efficacy.[11]

Previous studies investigating the effect of particle size on cellular uptake have predominantly focused on relatively small NPs <500 nm in diameter. Due to steric limitations, NPs size often dictates the uptake pathway, generally leading to reduced internalization of larger particles.[12] Most of them are internalized *via* endocytotic pathways like clathrin-mediated and caveolae-mediated endocytosis.[13,14] However, this size dependency is not always straightforward – it was demonstrated that extremely small 13 nm gold NPs showed decreased cellular uptake compared to 45 nm Au NPs.[15] Another interesting observation is the synergy of nanoparticles of different sizes on their cellular internalization.[16] It was shown that larger NPs with 100 nm diameter promoted the uptake of 50 nm ones and *vice versa*.

While size effects are important, particle stiffness has also emerged as a critical parameter influencing cellular uptake.[17] However, the interpretation of the results is complicated due to different cell lines and nature of NPs used in the experiment. Studies have shown that stiffer particles generally demonstrate enhanced uptake by macrophages.[18,19] For instance, studies with 300 nm gelatin NPs revealed that stiffer particles showed better internalization by dTHP1 and RAW 264.7 macrophages.[20]

The reduced uptake of softer particles has been attributed to their ability to deform during the internalization process, which may either complicate membrane passage or determine the endocytotic pathway.[21,22] At the same time, soft lysozyme–dextran NPs demonstrated deformability, which allowed them to penetrate caveolae sterically inaccessible to hard particles of the same size.[23]

While in addition to size and stiffness, other parameters such as surface chemistry, charge, and functional groups influ-

[a]*Institute of Physical Chemistry, RWTH Aachen University, Landoltweg 2, 52056 Aachen, Germany. E-mail: wrichtering@pc.rwth-aachen.de*
[b]*Department of Chemosensation, Institute of Biology II, RWTH Aachen University, Worringerweg 3, 52074 Aachen, Germany*

ence uptake, our present study focuses on the influence of particle softness and the influence of charges warrant separate investigations.[10,24,25]

In addition to NPs, microgels represent a distinct and promising class of delivery vehicles that offer several advantages over traditional NPs. These soft, hydrogel-based particles combine the benefits of both hydrogels and colloidal systems, exhibiting exceptional biocompatibility due to their high water content and polymeric nature.[26] Incorporation of different monomers during or post-synthesis allows tailoring pH-, light- or temperature-sensitive properties, adding to their versatility. Moreover, their inherent softness and deformability set them apart from rigid nanoparticles discussed above, potentially enabling unique cellular interaction mechanisms.

Our current knowledge reveals that similarly to rigid nanoparticles, microgel softness and size play a significant role in cellular internalization. Banquy *et al*. demonstrated that the softness of microgels determines their internalization pathway when exposed to macrophages RAW 264.725.[27] They investigated *N*,*N*-diethyl acrylamide and 2-hydroxyethyl methacrylate microgels (90% and 10% respectively) featuring cross-linking densities ranging from 1.7 to 15 mol% and diameters of 150–180 nm. Microgels with lower Young's moduli were internalized through macropinocytosis, while stiffer ones were taken up *via* clathrin-mediated endocytosis.

In our previous study, we further illustrated that HEK293T cells take up PNIPAM-based microgels within seconds to minutes.[28] Notably, small microgels with 5% and 15% cross-linking density were internalized, and remarkably, with 5% cross-linker content, even microgels with 1 μm diameter were taken up by cells – a size regime where rigid nanoparticles typically show no cellular entry. However, 1 μm size microgels with cross-linking contents of 10–15% did not penetrate the cells, suggesting a complex interplay between size and softness in determining cellular uptake.

In addition to microgels prepared with a dedicated cross-linker, PNIPAM can be synthesized without the addition of a cross-linking agent. Instead, the network forms through self-cross-linking of NIPAM due to transfer reactions.[29–31] The application of these ultra-low cross-linked (ULC) microgels is particularly intriguing due to their remarkably soft properties, which result in diverse behaviors during adsorption and deformation, thus expanding their potential biological applications.[32,33] For example, Nellenbach *et al*. utilized them to mimic platelets.[34] To enhance their blood-clotting function, the authors also modified ULC microgels with anti-fibrin antibodies, reducing the hydrodynamic radius from 1.5 μm to 0.5–0.8 μm. Interestingly, these modified microgels were not internalized by RAW 264.7 cells, but were predominantly observed on the extracellular surface of the cellular membrane.

Given these complex relationships between nanocarrier properties and cellular interactions, precise characterization of microgel mechanical properties is essential for creating designer nanomaterial. Atomic force microscopy (AFM) has emerged as a powerful tool that can be used for elasticity measurements,[35] nanorheology[36] and other kinds of soft matter characterization.[37,38] Force spectroscopy measurements with sharp tip offer nanoscale resolution enabling direct measurement of individual particle properties[39] under physiologically relevant conditions.

Our aim in this work was to employ AFM to investigate the correlation between microgel mechanical properties and their cellular uptake behavior, using HEK293T cells as our model system. These immortalized human embryonic kidney cells combine the practical advantages of an established cell line with behavior more representative of normal human cells compared to cancer-derived lines like (*e.g.* HeLa). Understanding these relationships will not only advance our fundamental knowledge of soft particle–cell interactions, but also guide the rational design of microgel-based drug delivery systems.

2. Experimental section

2.1. Microgel synthesis

All microgels were synthesized *via* precipitation polymerization. The main monomer *N*-isopropylacrylamide, *N*,*N*′-methylenbis(acrylamide) as a cross-linker, and methacrylic acid as a comonomer, were dissolved in degassed water and introduced into a three-neck round-bottom flask equipped with a mechanical stirrer, reflux condenser, and N_2 inlet. Methacryloxyethyl thiocarbamoyl rhodamine B was dissolved in degassed water *via* sonication and was added to the reaction mixture. Depending on the targeted size, the stirring speed and temperature were set to reaction conditions under N_2 atmosphere.

The reaction was started by adding previously dissolved initiator Potassium persulfate to the reaction flask and let to proceed for 4 h, if not stated otherwise. The reaction mixture was filtrated *via* glass wool and cooled down to room temperature. Purification was achieved either by three sets of centrifugation and replacement of the supernatant with double-distilled water (for large microgels) or by dialysis (for small microgels). The microgels were lyophilized for storage.

2.2. Sample preparation

The freeze-dried microgels were redispersed in water. Microscope slides were cleaned by ultrasonication in isopropanol, then the surface was activated in an ozone oven for 15 minutes. Subsequently, they were coated with poly(allylamine hydrochloride) (PAH). The samples were then dispensed onto the glass slides and processed either by spin-coating or by *in situ adsorption* at appropriate concentration. For the spin-coating, 120 μL of the mixed microgels solution was dropped onto the glass slide and it was rotated at a speed of 2500 rpm for 30 seconds. For the *in situ* adsorption 120 μL of the mixed microgel solution was applied to a glass slide and left for 1 hour to allow for adsorption. Subsequently, the slide was rinsed several times with 2 mL of Ringer's solution to remove any unabsorbed microgels (more information in S2 part of SI).

2.3. Atomic force microscopy (AFM)

Measurements were performed on a Dimension Icon AFM with a closed loop (Veeco Instruments Inc., software Nanoscope 9.4 (Bruker Corporation)). The measurements were recorded in the Peak Force QNM mode at 27 °C in Ringer's solution, using MSNL-10-E tip (Bruker) with a nominal resonance frequency of 38 kHz in air and a nominal spring constant of 0.1 N m^{-1} (radius: 2 nm, semi angle of the tip: 23°, assumed sample Poisson's ratio 0.3). Acquired data was processed using Nanoscope Analysis and a custom-made MATLAB script.[40] More information can be found in the SI. Ringer's solution: in mM: 145 NaCl, 10 HEPES, 5 KCl, 1 $CaCl_2$, 1 $MgCl_2$, pH 7.3 (±0.01), osmolarity 300 mOsm (±1).

2.4. Cell culture

All experiments were conducted with human embryonic kidney 293T (HEK293T) cells (ACC 635, DSMZ, Germany). Cells were cultivated in T75 flasks (Sarstedt AG, Germany) in a supplemented cell culture medium, consisting of Dulbecco's Modified Eagle Medium/Ham's Nutrient Mix F-12 + GlutaMAX (DMEM/F-12 + GlutaMAX; Gibco by Life Technologies, Thermo Fisher Scientific, USA) with 10% fetal bovine serum (FBS; Gibco by Life Technologies, Thermo Fisher Scientific, USA) and 1% penicillin and streptomycin (Pen/Strep; Gibco by Life Technologies, Thermo Fisher Scientific, USA) at 37 °C and a constant CO_2 level of 5%. For all experiments, cells were used at least 2 days after passaging to ensure proper adherence and habituation of the cells.

2.5. Confocal live-cell imaging of microgel uptake

Measurements were carried out using an inverted confocal laser scanning microscope (Leica TCS SP8) with HC PL APO 86×/1.20 water objective. Imaging was performed at 22 °C. For the internalization kinetics, it was done as following. After recording the baseline fluorescence signal, the microgel solution (0.5 mg mL^{-1}) was added and rate of uptake was measured over time. We tested concentrations in the range 0.16 to 1.5 g L^{-1}, see data in SI, showing the same general behavior. When low microgel concentrations were used, for S5% microgels complete uptake into cells was observed indicating that the limit of uptake was not reached. At the same time, ULC microgels at low concentrations produced insufficient fluorescent signal due to their extremely low density. Across all microgel types, 0.5 mg mL^{-1} was found to be optimal as it provides sufficient fluorescence signal, and saturation of microgel uptake is reached. Cells were imaged for 90 min at 1 frame per min, resulting in a total observation time of 1 h. Subsequently, using FIJI, the cell area excluding the nucleus was segmented for each cell, and the rate of relative fluorescence change (dF/F_0) was fitted using an exponential function with a characteristic time τ.[28]

For investigation of microgels distribution after internalization, additional STED module (Leica TCS STED X) was used with 775 nm pulsed STED laser. Nuclei and cell membrane were stained using a dye mixture of Hoechst 33342 and CellBrite. Immediately after internalization, the staining solution was washed in and incubated for 15 min at 37 °C. Using the UV-light (Hoechst 33342), 488 nm (CellBrite), 552 nm (rhodamine B) laser lines, the distribution of microgels was recorded.

2.6. Dynamic light scattering (DLS)

Microgels were measured in Ringer's solution at high dilution to prevent multiple scattering. The DLS measurements were contacted using an ALV goniometer setup equipped with a HeNe laser (λ = 633 nm), goniometer (ALV/CGS-8F), two avalanche photodiodes (PerkinElmer Inc. SPCM-CD2969), a digital hardware correlator (ALV 5000) and light scattering electronic (ALV/LSE-5003). A thermal bath filled with toluene was used to match the refractive index of the glass cuvettes. Temperature was controlled using a programmable thermostat. Measurements were performed at scattering angles from 30° to 110° in 10° increments. The initial decay rate Γ was derived from a first-order cumulant analysis of the normalized intermediate scattering function $f(q, t)$. The diffusion coefficient D was estimated from the q^2-dependence $\Gamma = Dq^2$, and the hydrodynamic radius R_{hyd} was obtained *via* the Stokes–Einstein relationship $D = k_B T/(6\pi\eta_s R_{hyd})$, where k_B, η_s, and T are the Boltzmann constant, solvent viscosity, and absolute temperature, respectively.[41]

2.7. Static light scattering (SLS)

Microgels were measured at 20 °C in Ringer's solution and were highly diluted to prevent multiple scattering. A temperature-regulated sample chamber within a closed goniometer manufactured by SLS-Systemtechnik GmbH was used. Measurements were conducted at a fixed wavelength of 640 nm with a range of 10° to 60° scattering angle using 1° increments. The data underwent background correction by subtracting buffer (solvent) scattering contributions. Intensity standardization was performed using toluene as a reference scattering material. Analysis of the SLS data was performed using MatLab-based FitIt! Software with fuzzy sphere and fuzzy sphere core shell models.[42,43]

3. Results and discussion

In this study, we investigated the relationship between microgel mechanical properties and cellular uptake behavior using AFM. We based our investigation on a well-characterized set of microgels that demonstrated varying cellular internalization behaviors in our previous work.[28]

We used small and large PNIPAM microgels co-polymerized with methacrylic acid (MAA) with different concentrations of cross-linker. The incorporation of methacrylic acid as a copolymer not only enhances colloidal stability in the presence of salt but also imparts pH sensitivity, presenting potential advantages for the design of delivery agents.[44] Additionally, while the volume phase transition temperature (VPTT) remains typical for PNIPAM at 32 °C, the swelling ratio in

Ringer's solution is smaller due to electrostatic screening (Fig. S1).

The microgels were synthesized in two size ranges – small (S) and large (L) – with cross-linker concentrations varying from 5% to 15% (Table 1). The MAA concentration was selected around 5% (for S15% is slightly higher – 8%). The cross-linker content and MAA concentration are given as molar percentage (mol%) used during synthesis. The hydrodynamic radius (R_{hyd}) and electrophoretic mobility were measured in Ringer's solution. The swelling ratio α is defined as the ratio between the hydrodynamic radii measured at 20 °C and 50 °C. Throughout this paper, samples are designated by size (S/L) followed by molar cross-linker percentage, used during synthesis (*e.g.*, S5% indicates small microgels with 5% cross-linker density).

Our previous work revealed a strong dependence of cellular uptake on both microgel size and cross-linking density. Cellular experiments conducted in Ringer's solution demonstrated distinct internalization patterns (Table 2). Small microgels (S5% and S15%) were readily internalized by HEK293T cells, with S5% showing the fastest uptake kinetics. Among larger microgels, only those with the lowest cross-linking density (L5%) achieved cellular entry, albeit at a slower rate than their smaller counterparts. Large microgels with cross-linker content above 10% were not internalized.[28]

These distinct patterns of cellular uptake suggested a complex relationship between microgel mechanical properties and their ability to enter cells. To elucidate this relationship, we employed AFM, which allows precise characterization of mechanical properties at the single-particle level under physiologically relevant conditions.

AFM provides unique capabilities for investigating the mechanical properties of microgels at the nanoscale.[36] Using force volume measurements, we can map the three-dimensional distribution of mechanical properties throughout individual microgel particles. The choice of the AFM probe is crucial for these measurements: large colloidal probes compress the microgel network, providing information about bulk elasticity and Young's modulus, while sharp cantilevers can penetrate between polymer chains, revealing local mechanical properties at high spatial resolution.[39] In our study, we employed sharp cantilevers to probe the internal structure of the microgels. As the tip penetrates the microgel, the resulting force–distance curves provide detailed information about local resistance to deformation. The first derivative of these curves, designated as contact stiffness, enables us to generate three-dimensional mechanical property maps (Fig. 1).

Table 1 Overview of the microgels used in this study, where α_{max} is the swelling ratio, R_{hyd} is hydrodynamic radius and El. mob is electrophoretic mobility

Paper sample code	Cross-linker, mol%	MAA, mol%	α_{max}	R_{hyd} (27 °C), nm	El. mob. 10^{-8} m^2 (V s)$^{-1}$
L5%	5	5	2.5	427	−0.29
L10%	10	5	1.9	501	−0.27
L12%	12	4	1.9	495	−0.51
L15%	15	5	3	463	−0.27
S5%	5	6	1.5	98	−0.44
S15%	15	8	2.3	127	−0.46

Table 2 Overview of the median characteristic times of internalization in seconds[28]

Sample code	S5%	S15%	L5%	L10%, L12%, L15%
Median time, s	732	1089	1610	No uptake

We initially employed spin-coating for AFM sample preparation given its several advantages. This method offers precise control over microgel surface density through adjustment of concentration and spinning parameters. Additionally, spin-coated samples can be stored and measured in both dry and rehydrated states. However, this approach has limitations. The drying process introduced artifacts through external forces that could stretch and deform microgels, potentially altering their mechanical properties. More critically, when attempting to measure S5% microgels, we found they consistently desorbed upon rehydration in the solution, making measurements impossible.

These challenges led us to apply an alternative approach using *in situ* adsorption.[32] While technically more demanding, this method allows microgels to maintain a structure that better represents their configuration during cellular interactions. All measurements were conducted in Ringer's solution to match our cellular experiments, maintaining physiological ionic strength and pH (7.3). Although technical constraints required a slightly elevated temperature (27 °C *versus* 22 °C used in cell experiments), both temperatures remain well below the VPTT of these microgels, ensuring comparable swelling states.

We initially focused on two types of large microgels that showed contrasting cellular uptake: L5%, which was internalized by cells, and L15%, which showed no uptake. Fig. 1 presents the contact stiffness profiles of these microgels prepared using both spin-coating and *in situ* adsorption methods. The preparation method significantly influenced the observed microgel properties. After spin-coating, both types of microgels appeared more compressed, showing reduced height and increased contact stiffness compared to *in situ* measurements. The effect was particularly pronounced for L5% microgels (Fig. 1A), which showed substantially more flattening than L15% (Fig. 1C), consistent with their lower cross-linking density. For *in situ* adsorption (Fig. 1B and D), while the overall compression was less pronounced, the distinctive mechanical properties of each microgel type were preserved. These differences are clearly reflected in the significant increase in stiffness along the Z axis, with L15% showing a steeper gradient. Notably, in all measurements, the central regions remained inaccessible to the AFM tip due to the force threshold set during the experiment, with L15% showing a larger inaccessible region indicative of its higher rigidity.

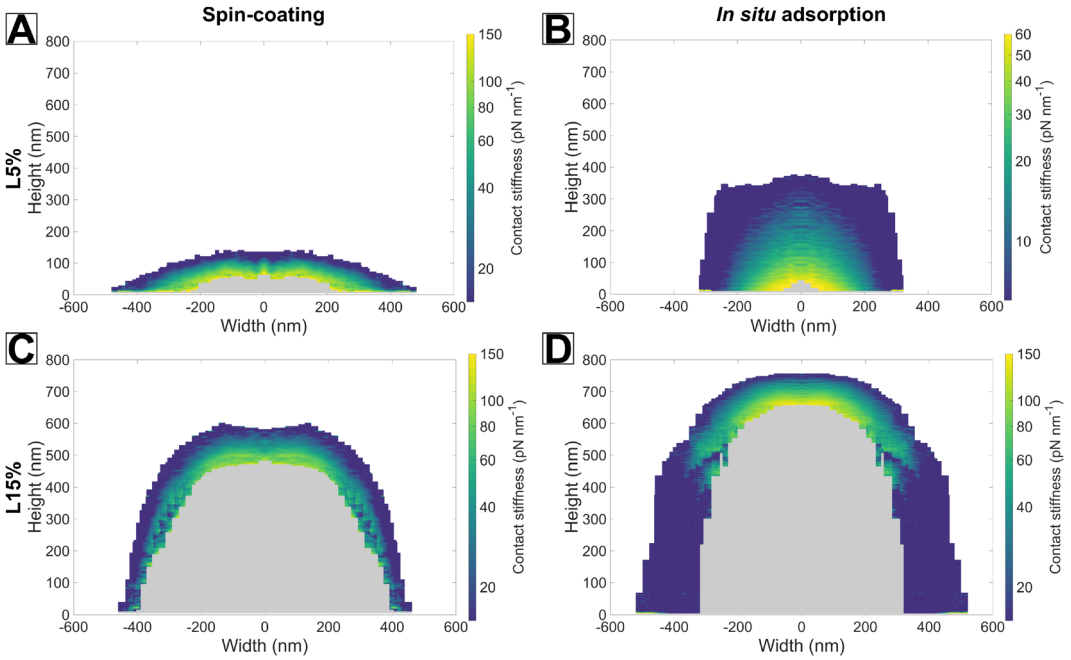

Fig. 1 Corresponding contact stiffness profiles through the center of the single microgel, measured in Ringer's solution at 27 °C on a PAH-functionalized glass substrate. Samples were prepared *via* spin-coating (A) L5%, (C) L15% and *via in situ* adsorption (B) L5%, (D) L15%. The color bar is 0–150 pN nm^{-1} for (A, C and D), 0–60 pN nm^{-1} for (B).

While contact stiffness profiles provided valuable insights into microgel mechanics, we aimed to identify additional parameters to quantitatively compare all microgel types. We selected two key parameters: vertical deformation and force–distance curves. Vertical deformation, defined as the ratio of height surface-adsorbed microgel to its diameter in bulk, provides information about particle softness and surface interactions. For an ideally undeformed sphere, this ratio equals 1, with increasing deformation resulting in lower values.

The comparison of vertical deformation revealed distinct patterns depending on the preparation method. For spin-coated samples, this parameter effectively distinguished between microgels with different cross-linker content (Fig. 2A), though S5% microgels could not be measured due to desorption during hydration. However, for *in situ* adsorbed microgels, the relationship between cross-linking density and deformation became more complex (Fig. 2B). Interestingly, we observed a trend where increasing vertical deformation corresponded to decreasing cellular uptake ability. This correlation was complicated by size effects: S15% microgels, despite showing intermediate internalization times between S5% and L5%, exhibited high vertical deformation similar to non-internalized large microgels. This size-dependent behavior can be attributed to surface interaction energies, which typically cause greater deformation in smaller microgels when comparing particles of similar stiffness.[45]

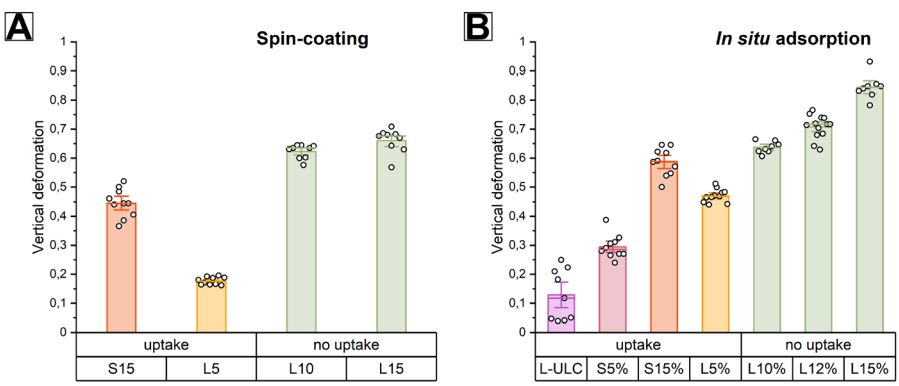

Fig. 2 Vertical deformation for microgels, measured in Ringer's solution at 27 °C on a PAH-functionalized glass substrate. Samples were prepared *via* spin-coating (A) and *via in situ* adsorption (B).

While vertical deformation provides useful insights within size-matched groups, we needed a more comprehensive parameter to compare microgels of different sizes. Force–distance curves, which measure the resistance encountered by the AFM tip as it penetrates the polymer network, proved to be particularly informative. Fig. 3 shows the averaged force–distance curves measured at the apex of each microgel type after *in situ* adsorption. For each microgel type, approximately ten individual microgels were measured, and their force–distance curves were averaged to obtain the representative curves. In these measurements, the zero point represents initial tip-microgel contact, with positive values indicating tip penetration depth. The differences between high and low cross-linked microgels were striking: under a 5 nN force, the AFM tip penetrated 300 nm into L5% microgels but only 80 nm into L15% microgels.

However, direct comparison of penetration depths was complicated by variations in microgels size. We addressed this limitation by normalizing the data, expressing penetration as a ratio of indentation to the height of the adsorbed microgel – termed "relative indentation" (Fig. 3B). This normalization revealed a remarkable correlation between mechanical properties and cellular uptake phenotype, clustering the microgels into three distinct groups:

- A "fast uptake" group (rightmost in the plot), comprising S5% microgels with the highest relative indentation and fastest cellular internalization.
- An "intermediate uptake" group, including L5% and S15% microgels, showing moderate relative indentation and slower but successful cell entry.
- A "no uptake" group (leftmost), containing large microgels with >10% cross-linking, characterized by low relative indentation and no cellular internalization.

This correlation between relative indentation and cellular uptake suggests that this normalized mechanical parameter could serve as a predictive indicator for microgel–cell interactions.

Having established a correlation between AFM-measured mechanical properties and cellular uptake, we sought to test this relationship using a new class of microgels. We synthesized large ultra-low cross-linked (ULC) microgels with acrylic acid. These microgels exhibit exceptionally high swelling ratios and pronounced sensitivity to ionic strength and pH changes, suggesting mechanical properties distinct from our previously studied systems.

Characterization of these ULC microgels using static light scattering (SLS) revealed their size and fuzzy sphere polymer distribution (Fig. 4A and B). Remarkably, despite having a hydrodynamic radius of 900 nm – far above the size typically associated with cellular uptake – these microgels demonstrated not only successful internalization but the fastest uptake kinetics observed in our studies, with a median internalization time of just 430 seconds (Fig. 4C). Fig. 4D shows a HEK293T cell after 1 hour of incubation with L-ULC (red) where we used an additional staining of the membrane. Fig. 4E and F show orthogonal projections from *z*-stack cell after incubation with L-ULC where the extracellular solution was labelled with membrane impermeable dye for additional contrast. These images reveal that the large L-ULC microgels were internalized and did not adsorb on the cell membrane.

To connect these unprecedented cellular behaviors with mechanical properties, we performed AFM characterization of ULC microgels (L-ULC). Based on previous work,[40] measuring such ultra-soft particles in their swollen state presented a significant challenge, as their extreme deformability typically renders them nearly 'invisible' to AFM. However, the combination of their large size (900 nm hydrodynamic radius) and negative surface charge enabled successful imaging and mechanical characterization.

Initial AFM measurements revealed heterogeneous surface behavior of L-ULC microgels (Fig. 5A), reflecting the exceptional softness of their polymer structure. During adsorption on glass/water interface heterogeneous stretching of their loosely crosslinked polymeric network can occur, leading to enhanced size polydispersity.[46] Individual microgels displayed significant variations in their surface-adsorbed conformations. Some of them exhibited extreme flattening, reaching contact

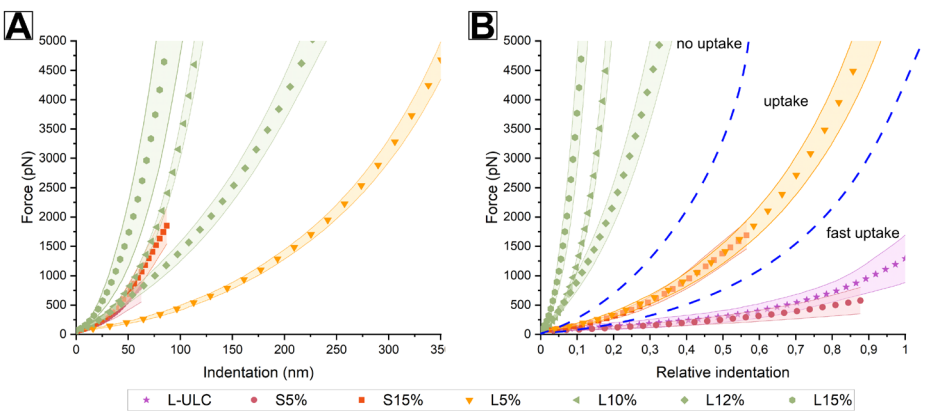

Fig. 3 Averaged force–distance curves corrected by the contact-point for the vertical approach of an AFM tip towards microgel's center. Microgels were measured in Ringer's solution at 27 °C on a PAH-functionalized glass substrate after *in situ* adsorption. Data are presented as (A) absolute indentation depth and (B) relative indentation normalized to the height of the adsorbed microgel.

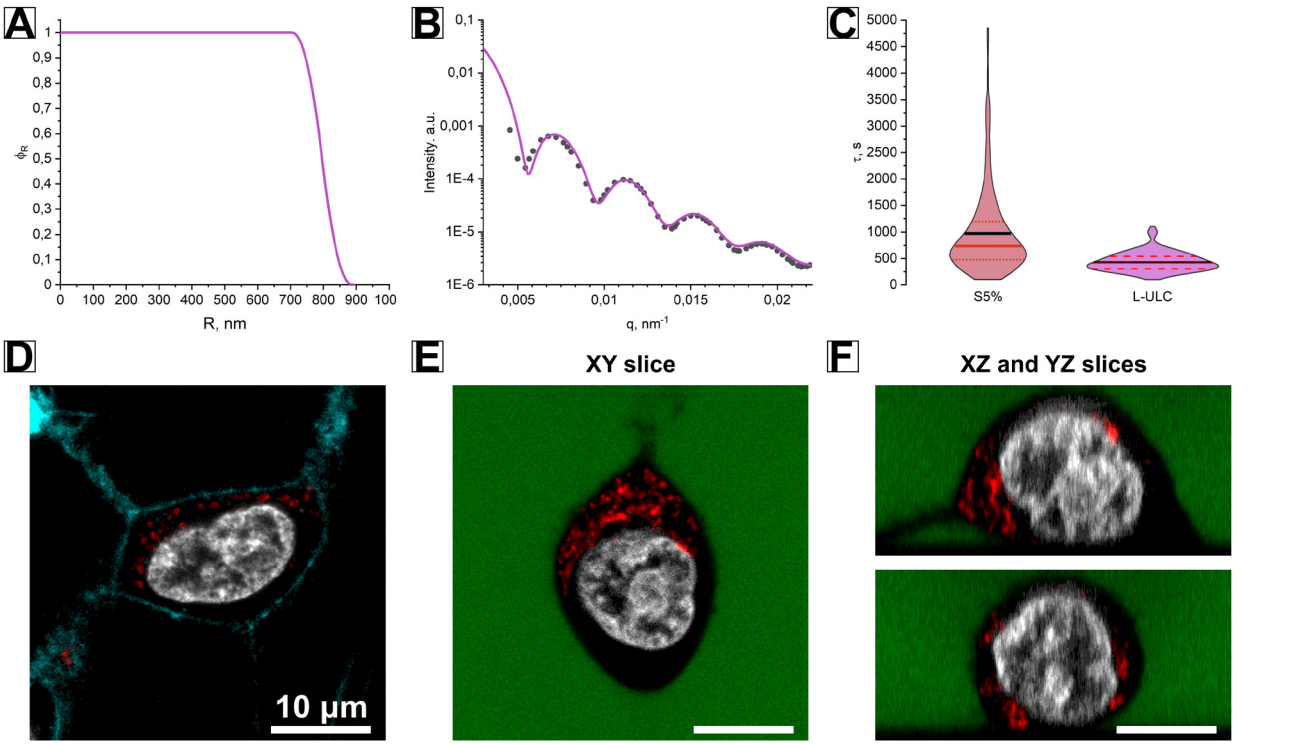

Fig. 4 (A) SLS form factor fitted with fuzzy sphere model at 20 °C in Ringer's solution. (B) Relative radial density profile obtained from fitting. (C) Comparison of the uptake kinetics for S5% and L-ULC microgels. Violin plots internalization time distributions: average (black line) and median (red line), dashed red lines show upper and lower quartiles. Data for S5% adapted with permission from ref. 26. (D) Typical image of a cell after 1 hour of incubation with L-ULC (red) with additional staining: membrane (cyan) and nucleus (grey). (E and F) Orthogonal projection from *Z*-stack of a cell after 1 hour of incubation with L-ULC (red) with additional extracellular solution (green) and nucleus (grey) stainings. The scalebar is 20 μm.

radii of up to 2 μm with heights as low as 50 nm, while others maintained a more hemispherical shape. This morphological diversity affected the force–distance measurements, resulting in variations between individual microgels (Fig. 5B). Despite this variability in absolute measurements, our relative indentation analysis effectively normalized these size variations and enabled meaningful comparisons across different microgel types. Remarkably, ULC microgels positioned themselves firmly in the "fast uptake" region of Fig. 3B, perfectly aligning with their rapid cellular internalization behavior. This striking correlation between AFM-derived mechanical parameters and cellular uptake kinetics provides compelling support for our analytical approach and suggests its potential predictive value for designing new microgel systems.

Internalization of various compounds is an essential mechanism in cellular life. Depending on their size, shape, softness and surface treatment, nanocarriers can enter cells through different pathways.[9,47] At the nanoscale (<200 nm), clathrin-dependent and caveolae-dependent pathways typically dominate, while larger objects primarily enter through macropinocytosis or phagocytosis. However, the relationship between size and uptake becomes more complex when considering highly deformable microgels. For example, Banquy *et al.* showed that the uptake of soft small microgels is significantly reduced after amiloride treatment, which inhibits macropinocytosis. While various pathway-specific inhibitors are commonly used to determine uptake mechanisms, this approach has limitations. Most inhibitors significantly modify cell physiology, potentially causing side effects (*e.g.*, cytotoxicity) and triggering compensatory uptake mechanisms. Genetic approaches, such as knockouts of specific proteins, can provide more definitive pathway identification. However, these advanced biological methods require extensive cell line modification and molecular biology techniques, which extend beyond the scope of our study. Instead, we focused on establishing the fundamental relationship between microgel mechanical properties and cellular uptake, providing a physical framework for future, more detailed biological investigations.

The combination of AFM and experiments on cellular uptake kinetics identified three distinct groups of microgels with characteristic uptake phenotypes. The first "fast uptake" group includes both the relatively small and soft S5% microgels and the extremely soft and large L-ULC microgels. Despite their significant size difference, both types demonstrate rapid internalization. AFM measurements reveal that both S5% and L-ULC microgels are exceptionally soft, with the cantilever encountering minimal resistance (not exceeding 2 nN, Fig. S1). This suggests that softness, rather than size, plays the dominant role in cellular uptake of these microgels, marking a significant difference from interactions with rigid nanoparticles.

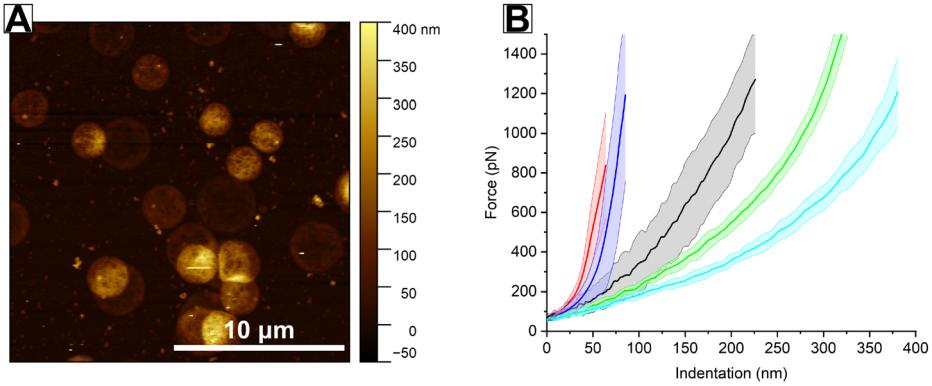

Fig. 5 AFM measurement of L-ULC microgels in Ringer's solution at 27 °C on a PAH-functionalized glass substrate after *in situ* adsorption. (A) Height image in scanning mode. (B) Force–distance curves of individual L-ULC microgels corrected by the contact-point for the vertical approach of an AFM tip towards microgel's center.

Previous studies with small nanoparticles (<200 nm) have shown that increased stiffness typically enhances cellular uptake,[18–20] One possible explanation is that soft particles tend to flatten against the cellular membrane, potentially increasing the energy barrier for complete membrane wrapping.[21] However, this mechanical limitation appears less critical for macropinocytosis, where rearrangement of the cytoskeleton forms large vesicles (0.2–5 µm macropinosomes) capable of internalizing substantial volumes.

The second "intermediate uptake" group comprises both stiff small (S15%) and soft large (L5%) microgels. For S15% microgels, successful internalization is not unexpected, as stiffness is not a major limitation for nanoscale objects. However, their increased cross-linking density reduces deformability, resulting in slower uptake compared to S5%. More notably, L5% microgels achieve cellular entry despite exceeding the typical size threshold (>500 nm) for non-phagocytic uptake. This suggests that in this intermediate regime, both size and stiffness modulate uptake kinetics, with increases in either parameter reducing internalization rates.

The third "no uptake" group consists of large microgels with high cross-linking density. Unlike L5%, these microgels exhibit minimal vertical deformation during surface adsorption, indicating limited deformability. This observation suggests that for micron-sized particles, deformability becomes a critical parameter that determines whether cellular internalization is possible at all.

The critical insights into the relationship between microgel softness and cellular uptake were made possible through our specific AFM approach using Force Spectroscopy with a sharp tip. In contrast to large colloidal probes, that are usually used for Young's modulus measurement, small sharp tip reveals local mechanical properties at nanoscale resolution. This method is particularly valuable for ultra-soft microgels like L-ULC, whose adsorption at interfaces is highly sensitive to changes in environmental conditions, resulting in diverse interfacial shapes and patterns.[48] The ability to resolve nanoscale mechanics ensures robust characterization of these responsive systems. Our experiments not only demonstrated a clear correlation between AFM-defined softness and cellular uptake but also revealed the remarkable ability of large ULC microgels (1.8 µm in diameter) to be internalized by cells. To our knowledge, this is the first demonstration of non-phagocytic uptake of nanocarriers of this size.[10,13,49] As HEK293T are not-phagocytic, only macropinocytosis is possible.

The involvement of specific uptake pathways is particularly interesting for drug delivery applications.[25] Many cancer cell types, including lung, pancreatic, and breast cancer cells, upregulate macropinocytosis to increase nutrient uptake from the tumor microenvironment.[50] Exploiting this pathway could enhance delivery specificity, potentially leading to more efficient treatment with fewer side effects. Additionally, recent studies also have shown that soft nanoparticles have prolonged blood circulation time, ability to penetrate deeper into the tumor and to avoid uptake by macrophages.[51–53] These findings significantly expand the potential biomedical applications of ULC microgels, particularly in targeted drug delivery systems.

4. Conclusions

The Force Spectroscopy measurements proved especially powerful, providing quantitative parameters that successfully predicted uptake behavior across our entire range of microgels, from highly deformable to relatively rigid microgels. In case of particularly soft polymer networks, size ceases to play a fundamental role, allowing the uptake of both small and large microgels. Moreover, micron-sized ULC microgels showed the remarkable ability for cellular uptake. In case of increased stiffness, the combination of size and softness begins to play a role, where increasing of either parameter reducing internalization rates. Thus, by manipulating the microgels size and stiffness, the specific features of microgel–cell interactions can be reached. These results will be a useful tool for the future design of therapeutic agents.

Author contributions

A. B. and W. R. developed the concept. A. B. carried out the experiments and evaluated the data. V. S. performed cell experiments. A. B. wrote the manuscript with support from V. S., M. S., and W. R. All authors reviewed the manuscript.

Conflicts of interest

There are no conflicts to declare.

Data availability

Data are stored according to the guidelines of the DFG. Data supporting this article (information about microgel synthesis and characterization, and detailed descriptions of AFM experimental conditions) have been included as part of the SI. See DOI: **https://doi.org/10.1039/d5nr02681d**.

Evaluated data are available at **https://dx.doi.org/10.22000/du95kb342kbsc23e**. Raw data (*e.g.* AFM files) are available upon request.

Acknowledgements

We acknowledge financial support from the Deutsche Forschungsgemeinschaft (DFG) for within the Sonderforschungsbereich SFB 985 "Functional Microgels and Microgel Systems". The authors acknowledge Alan Francisco Mejia for providing the ULC microgels and Christoph Hamacher for his help with STED microscopy.

References

1 S. A. Dilliard and D. J. Siegwart, *Nat. Rev. Mater.*, 2023, **8**, 282–300.
2 M. Karg, A. Pich, T. Hellweg, T. Hoare, L. A. Lyon, J. J. Crassous, D. Suzuki, R. A. Gumerov, S. Schneider, I. I. Potemkin and W. Richtering, *Langmuir*, 2019, **35**, 6231–6255.
3 G. Agrawal and R. Agrawal, *Small*, 2018, **14**, 1801724.
4 P. Agnihotri, D. Dheer, A. Sangwan, V. C. Chandran, N. A. Mavlankar, G. Hooda, D. Patra and A. Pal, *Nanoscale*, 2024, **16**, 19254–19265.
5 K. Obst, G. Yealland, B. Balzus, E. Miceli, M. Dimde, C. Weise, M. Eravci, R. Bodmeier, R. Haag, M. Calderón, N. Charbaji and S. Hedtrich, *Biomacromolecules*, 2017, **18**, 1762–1771.
6 M. Deloney, K. Smart, B. A. Christiansen and A. Panitch, *J. Controlled Release*, 2020, **323**, 47–58.
7 W. Richtering, I. Alberg and R. Zentel, *Small*, 2020, **16**, 2002162.
8 S. Boesveld, Y. Kittel, Y. Luo, A. Jans, B. Oezcifci, M. Bartneck, C. Preisinger, D. Rommel, T. Haraszti, S. P. Centeno, A. J. Boersma, L. De Laporte, C. Trautwein, A. J. C. Kuehne and P. Strnad, *Adv. Healthcare Mater.*, 2023, **12**, 2300695.
9 S. Zhang, H. Gao and G. Bao, *ACS Nano*, 2015, **9**, 8655–8671.
10 M. S. de Almeida, E. Susnik, B. Drasler, P. Taladriz-Blanco, A. Petri-Fink and B. Rothen-Rutishauser, *Chem. Soc. Rev.*, 2021, **50**, 5397–5434.
11 S. Wilhelm, A. J. Tavares, Q. Dai, S. Ohta, J. Audet, H. F. Dvorak and W. C. W. Chan, *Nat. Rev. Mater.*, 2016, **1**, 1–12.
12 F. Lu, S.-H. Wu, Y. Hung and C.-Y. Mou, *Small*, 2009, **5**, 1408–1413.
13 J. Rejman, V. Oberle, I. S. Zuhorn and D. Hoekstra, *Biochem. J.*, 2004, **377**, 159–169.
14 T. Wang, L. Wang, X. Li, X. Hu, Y. Han, Y. Luo, Z. Wang, Q. Li, A. Aldalbahi, L. Wang, S. Song, C. Fan, Y. Zhao, M. Wang and N. Chen, *ACS Appl. Mater. Interfaces*, 2017, **9**, 18619–18625.
15 T. Mironava, M. Hadjiargyrou, M. Simon, V. Jurukovski and M. H. Rafailovich, *Nanotoxicology*, 2010, **4**, 120–137.
16 L. Li, W.-S. Xi, Q. Su, Y. Li, G.-H. Yan, Y. Liu, H. Wang and A. Cao, *Small*, 2019, **15**, 1901687.
17 P. Gurnani, C. Sanchez-Cano, H. Xandri-Monje, J. Zhang, S. H. Ellacott, E. D. H. Mansfield, M. Hartlieb, R. Dallmann and S. Perrier, *Small*, 2022, **18**, 2203070.
18 Y. Hui, X. Yi, D. Wibowo, G. Yang, A. P. J. Middelberg, H. Gao and C.-X. Zhao, *Sci. Adv.*, 2020, **6**, eaaz4316.
19 X. Ma, X. Yang, M. Li, J. Cui, P. Zhang, Q. Yu and J. Hao, *Langmuir*, 2021, **37**, 11688–11694.
20 M. Yildirim, A.-V. Weiss and M. Schneider, *Pharmaceutics*, 2023, **15**, 199.
21 X. Yi, X. Shi and H. Gao, *Phys. Rev. Lett.*, 2011, **107**, 098101.
22 Y. Li, X. Zhang and D. Cao, *Nanoscale*, 2015, **7**, 2758–2769.
23 J. W. Myerson, B. Braender, O. Mcpherson, P. M. Glassman, R. Y. Kiseleva, V. V. Shuvaev, O. Marcos-Contreras, M. E. Grady, H.-S. Lee, C. F. Greineder, R. V. Stan, R. J. Composto, D. M. Eckmann and V. R. Muzykantov, *Adv. Mater.*, 2018, **30**, 1802373.
24 A. M. Bannunah, D. Vllasaliu, J. Lord and S. Stolnik, *Mol. Pharm.*, 2014, **11**, 4363–4373.
25 V. T. Cong, J. L. Houng, M. Kavallaris, X. Chen, R. D. Tilley and J. J. Gooding, *Chem. Soc. Rev.*, 2022, **51**, 7531–7559.
26 A. Scotti, M. F. Schulte, C. G. Lopez, J. J. Crassous, S. Bochenek and W. Richtering, *Chem. Rev.*, 2022, **122**, 11675–11700.
27 X. Banquy, F. Suarez, A. Argaw, J.-M. Rabanel, P. Grutter, J.-F. Bouchard, P. Hildgen and S. Giasson, *Soft Matter*, 2009, **5**, 3984–3991.
28 V. K. Switacz, S. K. Wypysek, R. Degen, J. J. Crassous, M. Spehr and W. Richtering, *Biomacromolecules*, 2020, **21**, 4532–4544.
29 J. Gao and B. J. Frisken, *Langmuir*, 2003, **19**, 5212–5216.
30 J. Gao and B. J. Frisken, *Langmuir*, 2005, **21**, 545–551.
31 M. Brugnoni, A. C. Nickel, L. C. Kröger, A. Scotti, A. Pich, K. Leonhard and W. Richtering, *Polym. Chem.*, 2019, **10**, 2397–2405.

32 M. F. Schulte, A. Scotti, M. Brugnoni, S. Bochenek, A. Mourran and W. Richtering, *Langmuir*, 2019, **35**, 14769–14781.
33 A. C. Brown, S. E. Stabenfeldt, B. Ahn, R. T. Hannan, K. S. Dhada, E. S. Herman, V. Stefanelli, N. Guzzetta, A. Alexeev, W. A. Lam, L. A. Lyon and T. H. Barker, *Nat. Mater.*, 2014, **13**, 1108–1114.
34 K. Nellenbach, E. Mihalko, S. Nandi, D. W. Koch, J. Shetty, L. Moretti, J. Sollinger, N. Moiseiwitsch, A. Sheridan, S. Pandit, M. Hoffman, L. V. Schnabel, L. A. Lyon, T. H. Barker and A. C. Brown, *Sci. Transl. Med.*, 2024, **16**, eadi4490.
35 Y. Liu, I. Sokolov, M. E. Dokukin, Y. Xiong and P. Peng, *Nanoscale*, 2020, **12**, 12432–12443.
36 S. Backes and R. Von Klitzing, *Polymers*, 2018, **10**, 978.
37 R. Geisler, M. A. Hormozi and R. von Klitzing, *Curr. Opin. Colloid Interface Sci.*, 2024, **69**, 101769.
38 A. Aufderhorst-Roberts, D. Baker, R. J. Foster, O. Cayre, J. Mattsson and S. D. Connell, *Nanoscale*, 2018, **10**, 16050–16061.
39 M. Friederike Schulte, E. Izak-Nau, S. Braun, A. Pich, W. Richtering and R. Göstl, *Chem. Soc. Rev.*, 2022, **51**, 2939–2956.
40 M. F. Schulte, S. Bochenek, M. Brugnoni, A. Scotti, A. Mourran and W. Richtering, *Angew. Chem., Int. Ed.*, 2021, **60**, 2280–2287.
41 W. Burchard and W. Richtering, *Progr. Colloid Polym. Sci.*, 1989, **80**, 151–163.
42 O. L. J. Virtanen, A. Mourran, P. T. Pinard and W. Richtering, *Soft Matter*, 2016, **12**, 3919–3928.
43 O. Virtanen, *Ovirtanen/Fitit*, 2022.
44 S. Zhou and B. Chu, *J. Phys. Chem. B*, 1998, **102**, 1364–1371.
45 K. L. Johnson, K. Kendall and A. D. Roberts, *Proc. R. Soc. London, Ser. A*, 1971, **324**, 301–313.
46 A. Scotti, S. Bochenek, M. Brugnoni, M.-A. Fernandez-Rodriguez, M. F. Schulte, J. Houston, A. P. Gelissen, I. I. Potemkin, L. Isa and W. Richtering, *Nat. Commun.*, 2019, **10**, 1418.
47 J. J. Rennick, A. P. R. Johnston and R. G. Parton, *Nat. Nanotechnol.*, 2021, **16**, 266–276.
48 H. Bachman, A. C. Brown, K. C. Clarke, K. S. Dhada, A. Douglas, C. E. Hansen, E. Herman, J. S. Hyatt, P. Kodlekere, Z. Meng, S. Saxena, M. W. Spears Jr, N. Welsch and L. A. Lyon, *Soft Matter*, 2015, **11**, 2018–2028.
49 I. Canton and G. Battaglia, *Chem. Soc. Rev.*, 2012, **41**, 2718–2739.
50 G. Lambies, S.-W. Lee, K. Duong-Polk, P. Aza-Blanc, S. Maganti, C. M. Galapate, A. Deshpande, A. J. Deshpande, D. A. Scott, D. W. Dawson and C. Commisso, *Nat. Commun.*, 2024, **15**, 10541.
51 Y. Hui, D. Wibowo, Y. Liu, R. Ran, H.-F. Wang, A. Seth, A. P. J. Middelberg and C.-X. Zhao, *ACS Nano*, 2018, **12**, 2846–2857.
52 A. C. Anselmo, M. Zhang, S. Kumar, D. R. Vogus, S. Menegatti, M. E. Helgeson and S. Mitragotri, *ACS Nano*, 2015, **9**, 3169–3177.
53 X. Chen, S. Zhang, J. Li, X. Huang, H. Ye, X. Qiao, Z. Xue, W. Yang and T. Wang, *Adv. Sci.*, 2022, **9**, 2202644.